Electronic Spectra and Transition Moments of 6-(2′-Pyridiniumyl)phenanthridinium Photoactive DNA Intercalators

Gonzalo Colmenarejo,*,† Anders Holmén,‡ and Bengt Nordén‡

Departamento de Bioquímica y Biología Molecular I, Universidad Complutense de Madrid, E-28040 Madrid, Spain, and Department of Physical Chemistry, Chalmers University of Technology, S-41296 Gothenburg, Sweden

Received: November 5, 1996; In Final Form: April 17, 1997[⊗]

The electronic transitions giving rise to the UV−visible absorption spectra of two pyridinium−phenanthridinium viologens, 6,7-dihydropyrido[2′,1′:3,4]pyrazino[1,2-*f*]phenanthridinediium dication (**1**) and 7,8-dihydro-6*H*-pyrido[2′,1′:3,4][1,4]diazepino[1,2-*f*]phenanthridinediium dication (**2**), have been investigated with respect to energies, intensities, and transition moment directions. A combination of methods has been applied: UV−visible absorption, circular dichroism, magnetic circular dichroism, fluorescence anisotropy, linear dichroism in stretched poly(vinyl alcohol) films, and semiempirical molecular orbital calculations. For both drugs, the lowest energy absorption band, occurring around 400 nm, results from two separate transitions. The corresponding electric transition dipole moments lie in the phenanthridine plane and are polarized, respectively, in the direction of the pyridine moiety (the lower energy transition) and parallel to the phenanthridine long axis (the higher energy transition). Up to four additional different $\pi \rightarrow \pi^*$ transitions account for a second band that peaks at 250 nm; they show different polarizations within the phenanthridine plane. The lowest energy transition of the whole spectrum of both drugs corresponds to the promotion of an electron from the HOMO to the LUMO, which are molecular orbitals mainly localized in the phenanthridine and pyridine rings, respectively, thereby implying a charge transfer, upon excitation, from the phenanthridine toward the pyridine ring. The experimental and theoretical results are discussed in relation to the spectroscopic, redox, and photochemical properties of these drugs.

Introduction

N,*N*′-Dialkyl-6-(2′-pyridyl)phenanthridine compounds comprise an interesting novel group of chiral photoactive drugs targeted to nucleic acids (Figure 1).[1−4,6,7] As derivatives of *N*,*N*′-dialkyl-2,2′-bipyridine, they belong to the family of organic dications called *viologens*, widely used as oxidants in chemistry and biology due to their ability to participate in reversible redox reactions.[5] Their general structure (Figure 1) also resembles that of the well-known DNA- and RNA-intercalator ethidium. Their high-affinity interaction with DNA has been shown to arise from an intercalative binding mode,[1] mainly driven by the polyelectrolyte term of the binding free energy, and with preference for alternating GC base pairs.[6] Due to their chiral nature, originating from the existence for each drug of two minimum-energy atropisomeric conformations with opposite pyridine orientations (*S* and *R*, see Figure 1), enantiospecific interactions with DNA were initially proposed based on molecular mechanics calculations[1] and have indeed recently been experimentally demonstrated.[3,6] The isolation of the pure enantiomers has been possible for the inversion-stable member **2** by using cellulose−DNA affinity chromatography.[3] These drugs show luminescence ($0.06 < \Phi_{em} < 0.20$), and at room temperature the emission comes from the radiative deactivation of a singlet excited state.[1] Contrary to the case of ethidium, their fluorescence is completely quenched by DNA instead of being enhanced.[1] From laser flash photolysis experiments, in combination with spectroelectrochemical measurements, an

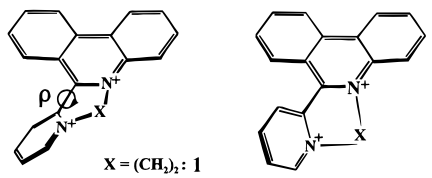

Figure 1. General structure of the pyp viologens studied showing the two enantiomeric conformations (*S* and *R*) observed for each member. The ρ torsion angle between the pyridine and phenanthridine planes is also depicted (previous AM-1 geometry optimizations gave values of $\rho = \pm 33°$ and $\pm 57°$ for **1** and **2**, respectively[1]). A third member of the series, **3**, previously described and not studied experimentally in this work (6-(1-methylpyridine)-5-methylphenanthridinediium dichloride hemihydrate), is characterized by possessing two methyl groups as quaternizing substituents, and a ρ angle of $\pm 94°$.[1]

electron transfer from the bases to the drug singlet excited state has been demonstrated to be responsible for the quenching mechanism.[4] This photooxidation has been proposed as the initial step in the mechanism of the photosensitized DNA cleavage that is demonstrated by these drugs, a conclusion based on the negligible effects that sodium azide, superoxide dismutase, and catalase (all quenchers of singlet oxygen, superoxide anion, and oxygen peroxide, respectively) have in the cleavage reaction.[2]

Due to the crucial importance of the excited states of these drugs for their photoactivity, a closer study of the nature of the electronic transitions that give rise to them was judged necessary in order to get a deeper understanding of the underlying photophysics. This study will also help to clarify the rich photophysics and photochemistry observed for these drugs when bound to DNA. Thus, the aim of this work has been to characterize the *electronic transition moments* and *excited states*

* Corresponding author. Present address: Department of Chemistry, University of California at Berkeley, and Structural Biology Division, Lawrence Berkeley National Laboratory, Berkeley, CA 94720.
† Universidad Complutense de Madrid.
‡ Chalmers University of Technology.
⊗ Abstract published in *Advance ACS Abstracts,* June 1, 1997.

S1089-5647(96)03702-9 CCC: $14.00

of two pyridinium−phenanthridinium compounds, namely **1** and **2** (Figure 1), by means of a combination of UV−visible absorption spectroscopy, circular dichroism (CD), magnetic circular dichroism (MCD), fluorescence anisotropy (FA), linear dichroism (LD) in poly(vinyl alcohol) stretched films, and semiempirical molecular orbital ZINDO calculations.

Materials and Methods

Chemicals. 6,7-Dihydropyrido[2′,1′:3,4]pyrazino[1,2-*f*]phenanthridinediium dibromide dihydrate (**1**) and 7,8-dihydro-6*H*-pyrido[2′,1′:3,4][1,4]diazepino[1,2-*f*]phenanthridinediium dibromide hydrate (**2**) were a gift from Prof. G. Orellana (Department of Organic Chemistry, Complutense University of Madrid, Spain). Their synthesis has been previously described,[7] but essentially it has followed the procedure of Petrow and Wragg[8] for the synthesis of 6-(2′-pyridyl)phenanthridine, with further quaternization of the nitrogen atoms following Hommer and Tomlinson.[9] For a thorough spectroscopic characterization and structural evidence, see ref 7. The two enantiomers of **2** were separated by affinity chromatography using a cellulose−DNA stationary phase (Sigma), as previously reported.[3] All experiments were conducted in 10 mM, pH 5.5 sodium phosphate buffer (P buffer), except when otherwise stated. Calf thymus DNA was isolated following Kay et al.[10] with further incubation with RNAse, pronase, and protein K, in order to completely eliminate any contaminating RNA or proteins; finally, sonication and exhaustive dialysis against P buffer was accomplished. Concentrations (in base pairs) of the polynucleotide were determined spectrophotometrically by using $\epsilon_{260} = 12\,800\ M^{-1}\ cm^{-1}$,[11] whereas for the drugs the previously reported absorption coefficients were used ($\epsilon_{387} = 8200\ M^{-1}\ cm^{-1}$ and $\epsilon_{366} = 9500\ M^{-1}\ cm^{-1}$ for **1** and **2**, respectively).[1] Ethylene glycol was standard p.a. quality. Poly(vinyl alcohol) (PVA) was obtained as powder from E. I. du Pont de Nemours Co. (Elvanol 71-30) and was refluxed in alkaline ethanol (in order to hydrolyze residual acetate) and washed in ethanol prior to use.

Film Preparation. PVA films were prepared by dissolving PVA in water heated from room temperature to 100 °C under vigorous stirring. Aliquots of 5 mL were mixed with 3 mL of an acidic (pH < 5, using sulfuric acid) aqueous stock solution of **1** or **2**, each containing 1 mg of substance. The mixtures were gently poured onto horizontal glass plates and left to dry in a dust-free environment. The films were removed with a spatula, clamped in a stretching device, and stretced to 2 times their original length in the hot air from a hair dryer.

Linear Dichroism (LD). The LD at a wavelength λ is defined as

$$\mathrm{LD}(\lambda) = A_{\parallel}(\lambda) - A_{\perp}(\lambda) \tag{1}$$

where $A_{\parallel}(\lambda)$ and $A_{\perp}(\lambda)$ are the absorbances measured with plane polarized light, parallel and perpendicular to the macroscopic sample axis (the stretching direction), respectively. The reduced linear dichroism, LD^{r}, is defined as

$$\mathrm{LD}^{\mathrm{r}}(\lambda) = (A_{\parallel}(\lambda) - A_{\perp}(\lambda))/A_{\mathrm{iso}}(\lambda) \tag{2}$$

where $A_{\mathrm{iso}}(\lambda)$ is the absorbance of a corresponding isotropic sample. For a uniaxial orientation of the sample molecules, such as in a stretched polymer matrix, $A_{\mathrm{iso}}(\lambda)$ can be calculated from the polarized components as[12]

$$A_{\mathrm{iso}}(\lambda) = (A_{\parallel}(\lambda) + 2A_{\perp}(\lambda))/3 \tag{3}$$

The chromophores studied in this work can be approximated to be planar structures, since most electronic transitions originate from molecular orbitals mainly located in the planar phenanthridinium ring system, or are of intramolecular charge transfer type with transfer from the phenanthridine moiety to the pyridine ring (see below). The effective shapes of these molecules are also planar as judged from the computed inertia moments. For a planar molecule, the LD^{r} of any pure in-plane polarized transition, *i*, can be related to the angle θ_i between the transition moment and the preferred molecular orientation axis, *z*, according to

$$\mathrm{LD}_i^{\mathrm{r}} = 3(S_{yy}\sin^2\theta_i + S_{zz}\cos^2\theta_i) \tag{4}$$

where the S_{yy} and S_{zz} are the Saupe orientation parameters for the in-plane (diagonal) axes *y* and *z*, respectively.[13] For an out of plane transition, the $\mathrm{LD}_i^{\mathrm{r}}$ is

$$\mathrm{LD}_i^{\mathrm{r}} = 3S_{xx} \tag{5}$$

For an in-plane polarized transition, the LD^{r} can have values between $3S_{zz}$ and $3S_{yy}$ (see eq 4)

$$3S_{yy} \le \mathrm{LD}_i^{\mathrm{r}}\ (\text{in-plane}) \le 3S_{zz} \tag{6}$$

and the orientation parameters are interrelated according to

$$S_{xx} + S_{yy} + S_{zz} = 0 \tag{7}$$

For overlapping transitions, the observed LD^{r} is a weighted average of the values of the $\mathrm{LD}_i^{\mathrm{r}}$ of the contributing transitions[14]

$$\mathrm{LD}^{\mathrm{r}}(\lambda) = \sum_i \epsilon_i(\lambda)\mathrm{LD}_i^{\mathrm{r}} / \sum_i \epsilon_i(\lambda) \tag{8}$$

where $\epsilon_i(\lambda)$ is the molar absorptivity associated with transition *i* at wavelength λ. In these cases, the pure reduced linear dichroism of each transition is determined by the so-called TEM method.[15,16] This method is based on forming linear combinations of the type $A_{\parallel} - dA_{\perp}$ with different values of the variation parameter, *d*. The value of *d* (d_i), for which a specific spectral feature disappears in the linear combination spectrum, is related to the LD^{r} of the transition *i* responsible for that feature by[17]

$$\mathrm{LD}_i^{\mathrm{r}} = 3(d_i - 1)/(d_i + 2) \tag{9}$$

Polarized UV measurements were performed on a Cary 4 Bio spectrophotometer with Glan-air space calcite polarizers in both the sample and reference beams. Five data points per nanometer were collected with a spectral bandwidth of 1 nm.

Gaussian Analysis of the Absorption Spectra. The two polarized absorption spectra in PVA films of each drug were simultaneously fitted to a sum of gaussians, assuming the same energy maxima and half width for each gaussian in both polarized spectra. For both **1** and **2**, a total of eight gaussians were used in order to account for all the experimental observations in the simplest way (see below).

Circular dichroism (CD) is defined as the differential absorption of left and right circularly polarized light

$$\mathrm{CD}(\lambda) = A_{\mathrm{l}}(\lambda) - A_{\mathrm{r}}(\lambda) \tag{10}$$

As both **1** and **2** are chiral molecules, their two corresponding atropisomers should exhibit opposite CD when isolated. Since the two enantiomers of **2** are inversion-stable at room temperature, their CD spectra can be measured separately. However, for **1**, whose interconversion at room temperature is fast,[3] the

CD was measured by adding to the racemic mixture of this compound an excess of DNA, which is itself chiral. The observed CD in this case is expected to be a composition of two contributions: (1) a net enrichment of the sample in the enantiomer preferred for binding to DNA (so-called Pfeiffer effect), given the enantiospecific interaction of this drug with the polynucleotide,[6] and (2) induced CD from interactions between the chirally positioned transition moments of the DNA bases and **1** (coupled oscillator mechanism).[18] A third mechanism (which may be regarded as induced CD) applies if the two enantiomers, by having different binding geometries, have differently perturbed absorption (and thus CD) intensities. All CD measurements were conducted at 25 °C on a JASCO J-720 spectropolarimeter with a Peltier-thermostated cell holder, using a spectral bandwidth of 1 nm, a response time of 1 s, a step resolution of 0.2 nm, and a scan speed of 100 nm/min.

Magnetic circular dichroism (MCD) spectra were recorded in the JASCO J-720 spectropolarimeter equipped with a permanent horseshoe magnet. Spectra of the racemic mixtures with both NS (north−south) and SN orientations of the magnetic field were measured. In order to eliminate any CD effects not originated from the magnetic field, the SN spectrum was subtracted from the NS one, and the result was divided by 2. The same procedure was accomplished for the P buffer, whose baseline was then subtracted from the previous spectrum. The gap between the magnetic poles was 2 mm, and the effective magnetic field was calibrated from the MCD signal at 510 nm of a standard 1 M $CoSO_4$ solution ($\Delta\epsilon = -1.88 \times 10^{-2}$ M^{-1} cm^{-1} T^{-1}).[19] The conditions for registration of spectra were the same as those of the CD experiments; 10 spectra were accumulated for each measurement in order to improve the signal-to-noise ratio.

Fluorescence anisotropy (FA) of the drugs was measured in an ethylene glycol/water (7/3 v/v) glass at 170 K using an AMINCO SPF-500 "corrected spectra" spectrofluorimeter equipped with a Glan polarizer in the excitation beam and a Polaroid film polarizer in the emission beam. Excitation spectra were recorded with both the excitation and the emission polarizers set either vertically (v) or horizontally (h). The emission intensity was monitored at 520 and at 495 nm, respectively for **1** and **2**. The FA spectra were then calculated from

$$\mathrm{FA}(\lambda) = (I_{vv}(\lambda) - I_{vh}(\lambda)G(\lambda))/(I_{vv}(\lambda) + 2I_{vh}(\lambda)G(\lambda)) \quad (11)$$

where $G(\lambda) = I_{hv}(\lambda)/I_{hh}(\lambda)$, a factor used for instrumental correction. In the formula above the first index subscript of the fluorescence intensity I refers to the excitation polarizer and the second one to the emission polarizer. For a pure transition i in a nonrotating molecule (within the fluorescence lifetime) the FA is given by[20]

$$\mathrm{FA}_i = 0.4(3\cos^2\xi_i - 1)/2 \quad (12)$$

where ξ_i is the angle between the absorption dipole moment of the transition i and the emission moment (in principle parallel to the first absorption transition dipole moment). For overlapping bands a method analogous to the TEM method is used, based on linear combinations of polarized intensities. The pure anisotropy is related to the reduction parameter d_i by[21]

$$\mathrm{FA}_i = (d_i - 1)/(d_i + 2) \quad (13)$$

Determination of the Orientation Parameters of the Drugs in the Stretched Films. The calculation of UV−vis transition moment directions from LD^r values using eq 4 requires first a determination of the orientation parameters S_{yy} and S_{zz}. To determine the in-plane parameters we use a method that is based on finding sets of S_{yy} and S_{zz} that satisfies both LD^r and FA measurements.[21] All possible combinations of S_{yy} and S_{zz} are generated, and for each combination the corresponding transition moment angles θ_i are calculated according to eq 4. The obtained transition moment angles are compared with those ξ_i determined from FA (eq 12) according to

$$\xi_i - \epsilon_i \le ||\theta_i(S_{yy},S_{zz})| \pm |\theta_1(S_{yy},S_{zz})|| \le \xi_i + \epsilon_i \quad (14)$$

where ϵ_i is the estimated inaccuracy, and θ_1 is the angle of the first transition. Orientation parameters that do not fulfill eq 14 neither for the sum nor for the difference of angles are discarded, leaving only a limited set of parameters consistent with experimental LD^r and FA values.

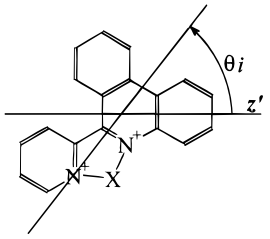

Figure 2. 6-(2′-Pyridiniumyl)phenanthridinium viologen drug with definition of the in-plane reference axis z'; as well as the in-plane angle θ_i relative to it.

Electronic Transition Moment Directions from Polarized UV−Vis Spectra and Fluorescence Anisotropy Measurements. A LD_i^r value provides information about the orientation of the ith transition with respect to the molecular axis which is on average best aligned, i.e. the molecular orientation axis z (eq 4). For the molecules studied in this work, we have no a priori knowledge of the direction of the molecular orientation axis. Experience from previous studies has shown that molecules oriented in stretched polymer films tend to orient with their smallest cross section perpendicular to the stretching direction.[22−24] On the basis of knowledge of the shape and the similarity between the molecules, it is then plausible to assume that the orientation axis z for both molecules is approximately identical to the z' reference axis shown in Figure 2, taking into account that the flexibility and the twist of the pyridinium ring makes this moiety less directing than the stiff phenanthridinium ring. This is in good agreement with what was found for the structurally related ethidium molecule.[25] Thus, in what follows, all the transition moment directions will be given as in-plane angles referred to the z' axis (Figure 2). Once the orientation parameters S_{yy} and S_{zz} were determined (see previous paragraph), the polarizations of the electronic transition moments relative to the molecular orientation axis were calculated using eq 4. The form of this equation implies that the polarized UV−vis measurements give two possible transition moment directions for each transition i, corresponding to angles with the same absolute value but with opposite signs. FA data can then be used to discard one of the two possible directions, since it gives the angle between the absorbing moment i and the emitting moment which is assumed to be parallel to the transition moment of the lowest lying transition.

Quantum Mechanical Calculations. The theoretical transition moment calculations were carried out with the ZINDO module of the InsightII 3.0.0 program (Biosym/MSI), run on an Indigo-2 Silicon Graphics workstation. For that purpose, self-consistent field configuration interaction (SCF/CI) calculations, using the semiempirical INDO/1 hamiltonian,[26] and adopting the Mataga−Nishimoto[27] scheme for the two-center

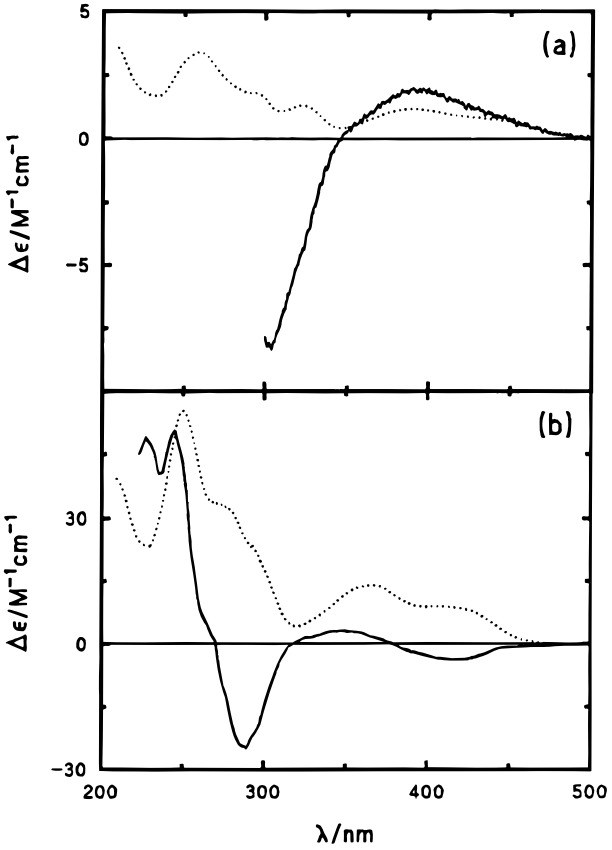

Figure 3. Absorption (···) and circular dichroism (—) spectra of **1** (a) and **2** (b) in P buffer. The CD of **1** was obtained with the (initially) racemic mixture of the drug in the presence of an excess of calf thymus DNA (drug/phosphate ratio = 0.085). The displayed **2** CD spectrum is that of the isolated enantiomer with higher DNA affinity.

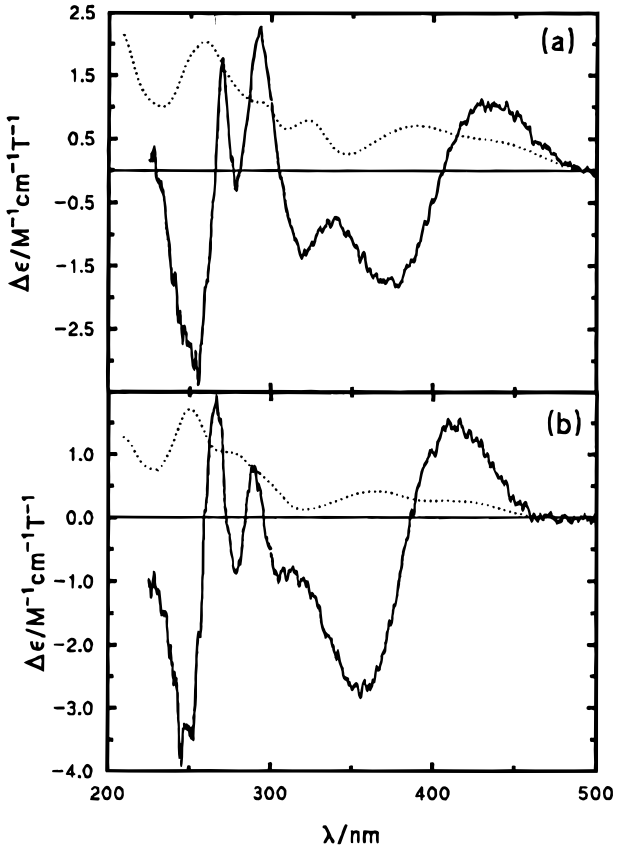

Figure 4. Magnetic circular dichroism (—) and absorption (···) spectra of the viologen drugs in P buffer: (a)**1**, (b) **2**.

electron repulsion integrals, were conducted. Two sets of configurations were used. The first one included 400 singly excited configurations. The second one included 530 singly excited configurations, together with 425 doubly excited configurations. Additionally, self-consistent reaction field calculations (SCRF/CI) were accomplished for each set of configurations, in order to simulate an aqueous environment surrounding the molecule. A dielectric constant of 78.5, a refractive index of 1.33, and a cavity radius generated from the mass density were used as conditions for these calculations. As input molecular geometries, the structures of the drugs optimized using the EF minimizator[28] with the AM-1 hamiltonian[29] (MOPAC 6.0 program) were used. Molecular orbital contours were calculated with the ZINDO program by generating a 25 × 25 × 25 point grid around the molecule extended 2 Å over the largest molecular sizes; the graphical interface of InsightII 3.0.0 was used for their visualization.

Results

Absorption, CD, MCD, FA, and LD^r spectra of **1** and **2** are displayed in Figures 3−6. As can be seen in these figures, qualitatively similar results are observed for the two drugs, differing only in the shift toward lower wavelengths of the **2** features with respect to **1**, particularly when considering the visible/near-UV region.

The absorption spectra of both drugs (Figure 3, dotted lines) show a band in the visible/near-UV region, which is absent in the closely related compound 6-(2′-pyridyl)phenanthridine (pyp) and in 2,2′-bipyridinium cations, as previously pointed out.[1] This band is broad, with a maximum at 387 and 366 nm, respectively, for **1** and **2**, and it presents a shoulder at its low-energy side. At lower wavelengths, another band is observed, displaying a maximum centered at about 250 nm, as well as different shoulders and local maxima at varying higher wavelengths depending on the compound. The 250 nm band is also observed in the pyp spectrum, but with a much higher intensity.[1] Finally, there is an absorption band peaking at approximately 200 nm.

The visible/near-UV CD spectrum of **1** bound to DNA in excess (Figure 3a) shows a positive peak at 390 nm and a negative one at 305 nm. The CD spectrum of one isolated enantiomer of **2** (the one preferred for DNA binding, Figure 3b) is bisignate in the visible/near-UV region, with a negative minimum at 420 nm, and a positive maximum at 355 nm; at shorter wavelengths a negative feature at 290 nm, and two positive maxima at 250 and 220 nm, are observed. The visible/near-UV region of this spectrum displays a red-shift and a hypodichroic effect when in the presence of DNA in excess (not shown).

Figure 4 shows that the MCD spectra of the racemic mixtures of both drugs are bisignate in the visible/near-UV region, with two lobes of similar magnitude. The (positive) maximum and (negative) minimum are centered at 430/415 and 375/355 nm, respectively, for **1**/**2**. At lower wavelengths a complex profile is observed, with multiple maxima and minima (see Figure 4a,b): in both spectra, two minima at nearly 280 and 250 nm, and two maxima at about 290 and 260 nm, are detected. There is also a negative minimum at 320 nm in the spectrum of **1** that seems to correspond to another one at 310 nm in the **2** spectrum, apparently overlapping the negative band centered at 355 nm.

The FA of the drugs in ethylene glycol/water glass at 170 K, displayed in Figure 5, is constant and near the upper limiting value of +0.4 in the region of the low-energy shoulder of the visible/near-UV band in the absorption spectra. A minor reorientation within the fluorescence lifetime, or a small direction difference between the emission and the absorption

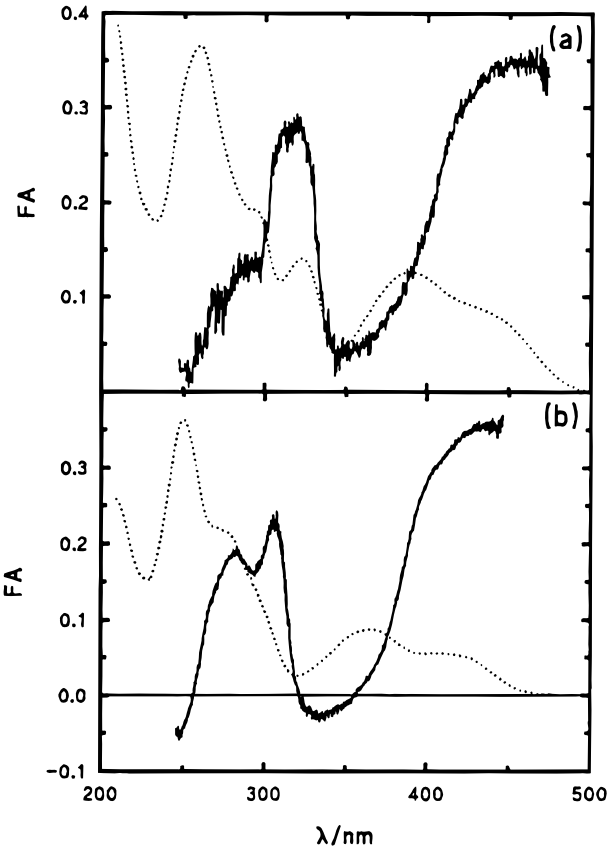

Figure 5. Fluorescence anisotropy (—) of **1** (a) and **2** (b) in ethylene glycol/water glass (7/3 v/v) and 170 K; the corresponding absorption profiles are also shown (···).

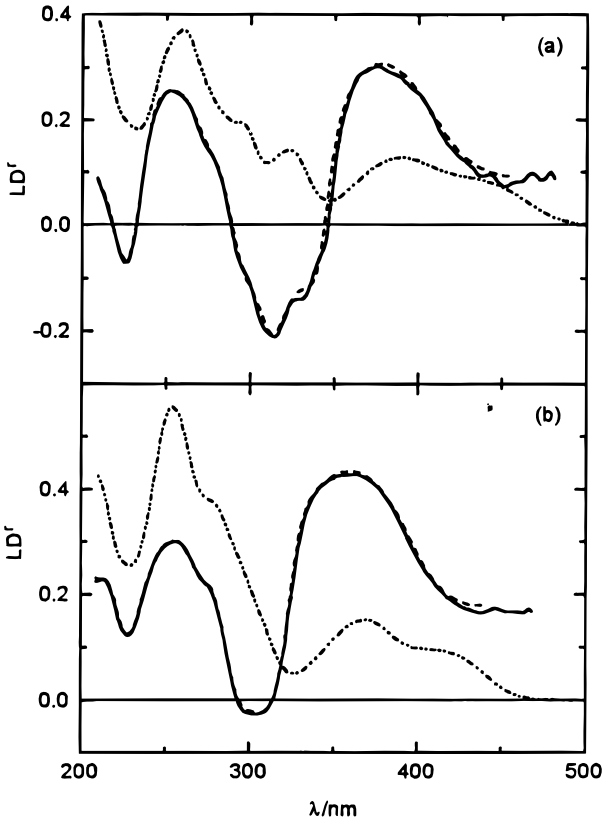

Figure 6. LDʳ spectra (—) of **1** (a) and **2** (b) in stretched PVA films; also shown are the corresponding absorption profiles (-···), as well as the predicted LDʳ (— — —) for the set of gaussians estimated in the fit of the polarized absorption spectra (see Discussion).

transition moments, could explain the value being slightly smaller than +0.4. At shorter wavelengths the FA goes down to approximately zero in the region of the visible/near-UV absorption maxima and then again increases, showing a dramatic variation with wavelength.

The LDʳ spectra of both drugs are displayed in Figure 6 (solid lines). There is a large change in the LDʳ when passing from the region of the shoulder (LDʳ ≈ 0.10 and 0.15 for **1** and **2**, respectively) to the maximum (LDʳ ≈ 0.30 and 0.45 for **1** and **2**, respectively) of the visible/near-UV absorption band. Two minima, at ∼310 and 225 nm, and one maximum, at ∼250 nm, are observed at lower wavelengths. Additional shoulders appear in this region that can be related with local maxima or shoulders in the corresponding absorption spectra.

The results of the quantum mechanical calculations are summarized in Table 1. Two transitions (I and II) at visible/near-UV wavelengths are predicted in all the calculations, for both **1** and **2**, that could account for the visible/near-UV absorption band. The lower energy one has a larger oscillator strength and is polarized roughly parallel to the bond connecting the pyridinium and the phananthridinium rings. For the second transition, a smaller oscillator strength is predicted. Its transition dipole moment is parallel to the long axis of the phenanthridine moiety, making an angle with the first transition moment of about 50°. Both calculated moments lie almost perfectly in the phenanthridine plane. The experimentally observed shift toward the blue of the visible/near-UV band when passing from **1** to **2** is successfully reproduced in all these calculations. The predicted energies appear generally to be lower than the experimental ones if only singly excited configurations are included in the CI; however, by including doubly excited configurations, the agreement between the experiment and the theory is considerably improved. Also in the second set of configurations, although the first transition still has a larger oscillator strength than the second one, the differences between them are smaller. If a reaction field is included in the SCF/CI calculation, the agreement of the energies is better when only singly excited configurations are included, but worse when including doubly excited configurations (Table 1, values in parentheses). From the inspection of the different configurations contributing to the excited states (not shown), it is concluded that the first transition in both drugs is virtually a HOMO → LUMO one, whereas the second excited state is mainly composed of a HOMO−1 → LUMO configuration. Molecular orbital contours (Figure 7) shows that the HOMO is mainly localized on the phenanthridine ring, whereas the LUMO has contributions from both the pyridine and the phenanthridine rings.

At higher energies multiple transitions are predicted (Table 1), polarized with a widespread distribution of directions, but still within a phenanthridine plane. The third transition in all the calculations is intense and polarized approximately perpendicular to the z' axis. Its wavelength is located between 281 and 331 nm, depending on the type of calculation. The corresponding excited state is mainly composed of the HOMO → LUMO+1 configuration. This last molecular orbital has a shape similar to the LUMO one, but with the signs inverted in the phenanthridinium moiety. Finally, there are also different high intensity transitions with wavelengths around 250 nm, as well as 220 nm, in accordance with the experimental spectra; their number, polarizations, and configurations compositions depend on the kind of calculation used.

Discussion

Two Electronic Transitions Are Responsible for the 350−500 nm Absorption of both 1 and 2. Taking into account

TABLE 1: Theoretical Transition Moments of 1 and 2[a]

	1			**2**		
transition	wavelength/nm	f_{osc}[b]	θ_i/deg[c]	wavelength/nm	f_{osc}[b]	θ_i/deg[c]
I	485(452)/452(418)	0.30/0.19	23/23	447(430)/416(398)	0.26/0.17	19/18
II	425(403)/394(371)	0.09/0.10	−31/−19	400(391)/368(358)	0.11/0.12	−33/−24
III	331(320)/316(299)	0.26/0.12	90/−82	330(307)/310(281)	0.10/0.05	−74/−73
IV	324/305	0.15/0.27	39/49	306/285	0.15/0.25	53/46
V	297/287	0.15/0.01	8/51	297/281	0.14/0.01	14/51
VI	282/279	0.00/0.02	−49/24	285/266	0.14/0.01	41/82
VII	280/274	0.13/0.06	65/−57	278/262	0.19/0.04	−48/−64
VIII	274/258	0.03/0.13	74/64	271/258	0.07/0.18	42/46
IX	271/255	0.47/0.27	−30/−18	264/252	0.30/0.33	−24/−27
X	250/245	0.33/0.01	−64/−23	251/241	0.48/0.13	−66/−56
XI	244/241	0.02/0.30	24/−42	246/238	0.08/0.15	−50/−48
XII	240/237	0.14/0.01	−58/42	239/232	0.02/0.01	−24/−35
XIII	235/227	0.01/0.05	−86/70	236/223	0.08/0.01	−59/−85
XIV	232/223	0.01/0.02	−10/−50	233/222	0.07/0.07	−33/−76
XV	231/218	0.04/0.06	37/−39	231/217	0.01/0.02	−36/−31
XVI	225/217	0.14/0.02	−29/−63	223/215	0.06/0.13	−58/−31
XVII	221/213	0.13/0.07	18/29	221/210	0.24/0.04	30/47
XVIII	216/209	0.13/0.04	47/26	215/206	0.02/0.05	17/48
XIX	214/207	0.11/0.04	−23/10	214/206	0.00/0.05	−27/41

[a] Values are shown for both **1** and **2**. For each column and transition, the first number corresponds to the SCF/CI calculations only including singly excited configurations, whereas the second one corresponds to the calculations including both singly and doubly excited configurations (see Materials and Methods). For the first three transitions, the wavelengths obtained from the SCRF/CI calculations are also included in parentheses. [b] Oscillator strength for the transitions. [c] Angle (with sign) between the transition moment and the proposed best orientation axis z′ (see Figure 2).

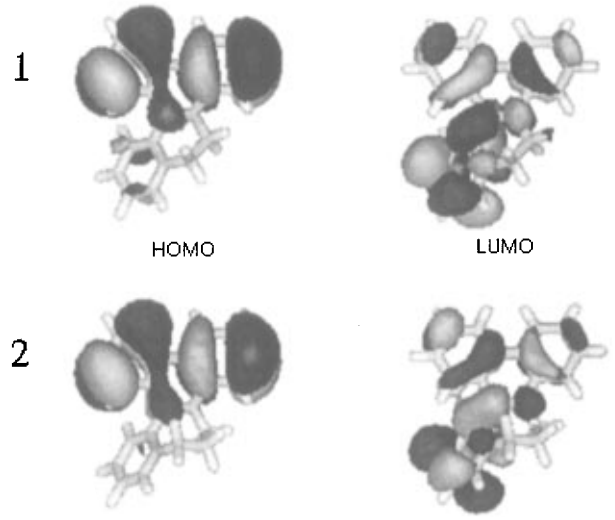

Figure 7. HOMO and LUMO contours (±0.03 amplitudes, positive in light gray and negative in dark gray) of **1** and **2**. The LUMOs+1 (not displayed) have similar shape than the LUMOs, but with the signs inverted in the phenanthridine moiety.

that the shape of a CD band due to a single transition should be similar to that of the corresponding absorption band (in the absence of vibronic or excitonic coupling with other transitions),[20] the bisignate appearance of the visible/near-UV CD spectrum of the isolated **2** enantiomer (Figure 3b) indicates that two different electronic transitions are responsible for its lowest energy absorption band. In the case of **1** bound to an excess of DNA, only a positive feature is observed at these wavelengths, but with a shape dissimilar to the corresponding absorption band (Figure 3a). Since the CD of this complex is expected to have an additional coupled oscillator component, no definitive conclusions from CD can be obtained about the number of transitions in this region for **1**. However, the corresponding MCD is bisignate, with two lobes of similar magnitude (Figure 4a). From perturbation theory, and considering the low symmetry of these molecules, their MCD is predicted to originate entirely from the so called B term.[12] The B terms of two transitions (0 → k and 0 → f) of near energy, and energetically well separated from other transitions are predicted to be of equal magnitude but with opposite signs, as given by[12]

$$B(0f) \approx (\nu_k - \nu_f)^{-1}\mathbf{m}(kf)\cdot[\mu(0k) \times \mu(0f)] \quad (15)$$

$$B(0k) \approx (\nu_f - \nu_k)^{-1}\mathbf{m}(fk)\cdot[\mu(0f) \times \mu(0k)] \quad (16)$$

where **m** and μ are the corresponding electric and magnetic transition dipole moments. Obviously, to get finite *B* terms the two electric transition moments have to be nonparallel. Then, following the strategy of assignment first described for the thiophene chromophore,[30] it is concluded that the visible/near-UV absorption band of **1** comprises two different electronic transitions, too, having different polarizations. The MCD of **2** is also bisignate (Figure 4b), confirming the previous conclusion from CD about two transitions.

The biphasic character of the FA and LD^r (Figures 5 and 6) of both drugs in this region lends further support to the existence of two nonparallel transitions in the visible/near-UV region. Since in all of these spectra the positions of the first and second bands/phases coincide with the shoulder and maximum in the corresponding absorption spectra, respectively, it is concluded that these two features originate from the two electronic transitions proposed and are not a result of vibrational structure.

Four Different Transitions Are Required to Account for the 250 nm-Centered Absorption Band. The unambiguous interpretation of the number and polarizations of the electronic transitions at shorter wavelengths is more problematic as a result of an extensive overlap between absorption bands that is evidenced in this region. One transition is expected at about 320 nm for **1**, and at 310 nm for **2**, respectively, considering a feature observed in all the MCD, FA, and LD^r spectra at these wavelength positions. This transition would give rise to the local maximum of the absorption spectrum of **1** located at 318 nm (Figure 3a). A common clear feature is also observed in all the spectra around 250 nm for both **1** and **2**. The corresponding transition would account for the main absorption maximum of both drugs at this wavelength (Figure 3a,b). Between these two transitions, the MCD and FA spectra show different maxima/minima, and in the LD^r a steady variation with a shoulder at ∼265 nm is detected. This indicates that there are at least two additional electronic transitions in this region.

TABLE 2: Experimental UV−Vis Transitions of 1/2

transition	λ/nm[a]	f_{osc}[b]	LD^r [c]	ξ_i/deg[d]	$\theta_i(\theta_1)$/deg[e]	sign[f]
I	443/421	0.051/0.056	0.097/0.17	0/0	64(0)/68(0)	+/+
II	387/367	0.16/0.18	0.31/0.43	50/52	57(59)/56(56)	−/−
III	323/303	0.091/0.080	−0.22/−0.025	21/29	82(18)/87(25)	+/−
IV	295/290	0.14/0.15	∼0/∼0	40/36	68(48)/82(30)	−/−
V	273/279	0.17/0.17	0.14/0.23	44/35	63(53)/65(47)	−/−
VI	255/254	0.37/0.71	0.26/0.30	52/59	59(57)/62(50)	−/−
VII	220/222	0.28/0.29	−0.07/0.12		72/72	
VIII[g]	∼200/∼208					

[a] Band maxima obtained from gaussian fit of the polarized absorption spectra in stretched PVA film. [b] Oscillator strengths calculated from $f_{osc} = 4.315 \times 10^{-9} \int \epsilon(\nu)\, d\nu$. [c] Values of LD^r obtained from TEM analysis of the polarized absorption spectra in stretched PVA film using the previous band maxima. [d] Angle between the ith transition moment and the emitting moment. Since the FA in the region of the lowest-energy transition is slightly smaller than 0.4, "effective" angles were calculated using $FA_i = FA_1(3\cos^2 \xi_i - 1)/2$, where FA_1 corresponds to the first transition moment. Below 250 nm there is absorption of ethylene glycol, so reliable FA data cannot be obtained at these wavelengths. [e] Angle between molecular orientation axis and the transition moment direction. Calculated from the LD^r value with eq 4 using $S_{zz} = 0.55$, $S_{yy} = -0.085$ for **1**, and $S_{zz} = 0.49$, $S_{yy} = -0.01$ for **2**. This gives an error in the estimated angles of no more than 5°. In parentheses, the angle between the corresponding transition moment and that of the first transition is shown (to be compared with the ξ values derived from FA, previous column). [f] Sign of the θ angle with respect to the molecular orientation axis (z' in Figure 2): counterclockwise (+), and clockwise (−). [g] Large number of gaussian parameter values gave fits of similar quality, so no accurate f_{osc} and LD^r can be given for this transition.

The shoulder at 293 nm of the **1** absorption spectrum (Figure 3a), and at 270 nm of the **2** one (Figure 3b), could be due to one of these transitions.

Band Maxima and Oscillator Strengths of the UV−Vis Transitions. In our interpretation above, a total of *six* electronic transitions had to be assumed to describe in the simplest way the 220−500 nm absorption of **1** and **2**. A sum of six gaussian components can then be used to fit the absorption spectrum of both drugs at these wavelengths, in order to estimate the energies and oscillator strengths of the proposed transitions. The use of gaussians can be justified by the absence of vibrational structure in both the CD and MCD spectra of the drugs, as well as by the fact that all local maxima and shoulders in the absorption spectra can be explained in terms of different electronic transitions (see above). Since both **1** and **2** also show a high intensity absorption band centered at ∼200 nm, it was necessary to use more than six gaussians in the fit of the whole spectra; in order to reproduce the variation in LD^r for the region between 200 and 220 nm, two additional gaussian components were included. The fit was made simultaneously with the two polarized absorption spectra (see Materials and Methods section). The eight estimated band maxima and oscillator strengths are collected in Table 2. The resulting sum isotropic absorption spectra, as well as their gaussian components, are shown in Figure 8 as short- and long-dashed lines, respectively; the experimental absorption spectra are also displayed therein as solid lines. In Figure 6 the theoretical LD^r spectra corresponding to these sets of gaussians are displayed as dashed lines, too. The observed excellent agreement with the experiment in both cases strongly supports the approach adopted. Additional confirmation comes from the coincidence of the estimated band maxima with features in both the FA and MCD spectra.

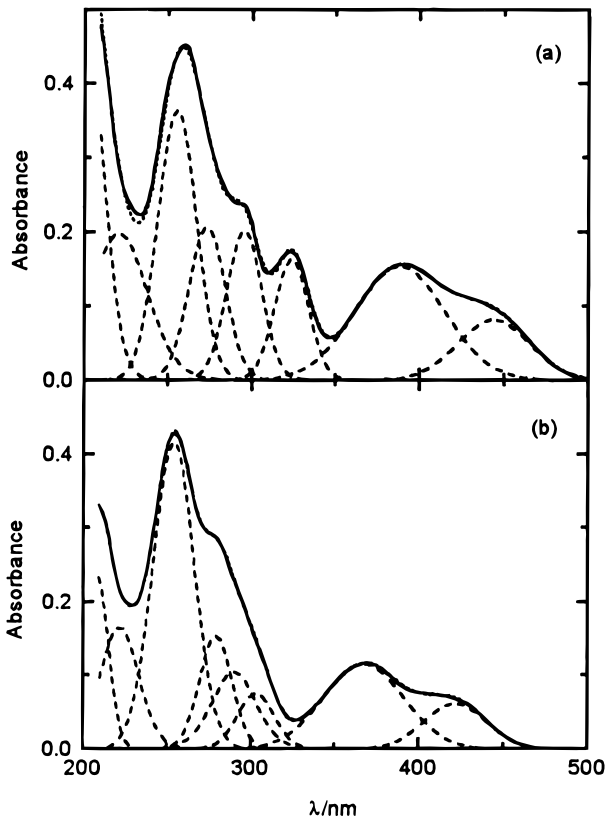

Figure 8. Gaussian fit of the absorption spectra of **1** (a) and **2** (b) in PVA stretched films. The experimental spectra (—) are shown for the two drugs, together with the corresponding calculated spectra (- - -) and the gaussian components (— — —).

Transition Moment Directions. Table 2 displays the LD^r values of the different proposed electronic transitions, derived from a TEM analysis using the previously derived band maxima (eq 9, see Materials and Methods). Also included in Table 2 are the FA-derived values of the angles ξ_i between the different absorption transition moments and the emission moment.

As explained in the Materials and Methods section, the transition moment directions of the viologen molecules can be approximated to lie in the phenanthridine plane, despite the fact that the absence of a symmetry plane in these compounds does not in principle exclude out of plane $\pi \rightarrow \pi^*$ intensity. This assumption is supported by the quantum mechanical calculations above described, where *all* transitions are almost perfectly polarized within this plane. This restriction simplifies the problem of the determination of the transition moments directions in three dimensions to the estimation of the angles θ_i between the different in-plane transition moments and the molecular orientation axis z (taken to be identical to the reference z' axis, see Materials and Methods), together with the corresponding sign.

In order to calculate the angles θ_i from the LD^r data by means of eq 4, knowledge of the orientation parameters S_{yy} and S_{zz} is required. These parameters can be estimated through the combination of the LD^r and FA information. Thus, for the different transitions, the angles θ_i are calculated with eq 4 for all the possible values of S_{yy} and S_{zz}; these angles are then compared with the FA-derived ones ξ_i by using eq 14. Only a very limited set of orientation parameters fulfill eq 14 simul-

taneously for all the electronic transitions. The resulting values for the viologen drugs are as follows: $S_{zz} = 0.55 \pm 0.05$ and $S_{yy} = -0.085 \pm 0.01$ for **1** ($\epsilon_i = 10°$), and $S_{zz} = 0.49 \pm 0.02$ and $S_{yy} = -0.01 \pm 0.005$ for **2** ($\epsilon_i = 15°$).

Once the orientation parameters are estimated, the θ_i angles can be calculated (eq 4): the resulting polarizations are collected in Table 2 for **1** and **2**. In order to discern between the two possible signs (+ or − θ_i), the ξ_i values were combined with the θ_i ones. The signs concluded are also shown in Table 2.

There is a reasonable agreement between these experimental transition moment directions and those obtained from the quantum mechanical calculations (compare Tables 1 and 2), particularly for the low-energy transitions. The first moment is approximately oriented toward the pyridine ring, while the second one is parallel to the phenanthridine long axis. The thrid moment makes an angle with the z' axis of +82° and −87° for **1** and **2**, respectively. These directions are in fair accordance with those obtained from the theoretical calculations (see Table 1) for the three first transitions. The agreement between observed and calculated oscillator strengths is worse and varies depending on the inclusion of doubly excited configurations and/or the consideration of the reaction field in the calculations. The best agreement in the energies (i.e. within 10 nm) is obtained in the calculation with doubly excited states without reaction field.

At wavelengths corresponding to the 250 nm band, the experimental absorption is dominated by transitions polarized nearly parallel to the phenanthridine long axis (between −59° and −68°, with one transition at −82°). The directions of the ZINDO moments of the main high intensity transitions corresponding to these energies display again reasonable agreement with experiment (between −18° and −64°, although there are also some transitions with positive angles). At shorter wavelengths (<250 nm) the theoretical calculations predict an increasing number of close lying transitions; no experimental directions can be obtained for this region due to the absence of FA data.

Origin of the Lowest Absorption Band. As previously pointed out,[1] neither *N*,*N*′-dialkylbipyridines nor 6-(2′-pyridyl)-phenanthridine (pyp) absorbs light in the visible region. The reason for a higher energy of the first transition in the first kind of molecules could be the smaller size of their aromatic system, since other viologen-like molecules generally having large aromatic rings (i.e. *N*,*N*′-dialkyldiazapyrenium and diazaperopyrenium dications) display absorption at longer wavelengths, too.[31−33] In an attempt to understand the appearance of visible absorption upon quaternizing the nitrogen atoms of the pyp molecule, further quantum mechanical calculations were performed, both on the separate moieties of this compound and those of the pyp viologens: pyridine and phenanthridine, with and withoug *N*-methyl groups, and for different ρ torsion angles and distances between them. In this way, the lowest energy transition properties of these molecules where found possible to model as the combined result of two effects: (a) HOMO−HOMO and LUMO−LUMO interactions of the two relatively uncoupled phenanthridine and pyridine moieties, which in turn depend on both the ρ angle of the molecule and the difference in the corresponding orbital energies and, (b) the effect of the electrostatic field of one moiety, when it is assigned a positive formal charge, on the orbital energies of the other one. With this approach, the pyridine HOMO and LUMO energies lie, respectively, well below and above the HOMO and LUMO energies of phenanthridine (Figure 9a). In the pyp molecule, where the low-energy conformation is characterized by the pyridine and phenanthridine rings being almost perpendicular

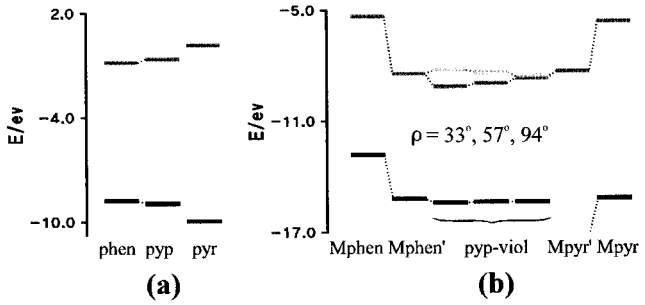

Figure 9. Orbital energies of the pyp molecule and the pyp viologens, as well as their separate moieties. Energies of HOMOs (black), LUMOs (dark gray), and LUMOs+1 (light gray) are shown: (a) phen, phenanthridine; pyp, 6-(2′-pyridyl)phenanthridine; pyr, pyridine; (b) Mphen, *N*-methylphenanthridine; Mphen', *N*-methylphenanthridine perturbed by the electrostatic field of a positive charge; pyp-viol, pyp viologens with different ρ angles; Mpyr', *N*-methylphenanthridine perturbed by the electrostatic field of a positive charge; Mpyr, *N*-methylphenanthridine.

(AM-1 calculations not shown), only minor molecular orbital interactions occur between these two moieties. Therefore, the resulting HOMO and LUMO of pyp correspond to the relatively unperturbed phenanthridine HOMO and LUMO, respectively (Figure 9a). The introduction of *N*-methyl substituents decreases the orbital energies of pyridine and phenanthridine (Mphen and Mpyr in Figure 9b), as expected from the generated positive charge. However, now the *N*-methylpyridine LUMO lie between the *N*-methylphenanthridine HOMO and LUMO. When these two moieties are brought together to form a pyp viologen molecule, the mutual influence of their electrostatic fields leads to a further decrease of the orbital energies (Mphen' and Mpyr' in Figure 9b), resulting in nearly degenerate LUMOs and a *N*-methylpyridine HOMO energy much lower than that of *N*-methylphenanthridine. Thus, in this case, the HOMO of the resulting molecule corresponds mainly to the *N*-methylphenanthridine HOMO (there are essentially no HOMO−HOMO interactions due to the large energy difference between these orbitals), whereas the LUMO and LUMO+1 are the "in-phase" and "out-of-phase" combinations of the two degenerate LUMOs, respectively (pyp-viol in Figure 9b). While the HOMO concerns only the phenanthridine part of the molecule, the LUMO extends over the whole structure (Figure 7), which explains the charge-transfer character of the lowest energy transition. This important displacement in the electronic density would provoke a large solvent reorientation upon excitation and thereby would account for the large Stokes shift observed for these drugs (ca. 120 nm).[1] Charge-transfer character is also expected for transitions II and III, since they are mainly composed of the HOMO−1 → LUMO and HOMO → LUMO+1 configurations, respectively (see Results), and the HOMO−1 is centered in the phenanthridine ring (not shown) while the LUMO+1 extends over the whole molecule (see above).

Within this picture, the visible absorption of the pyp viologens emerges from the generation of a low-energy LUMO in the combined system. The energy of this last molecular orbital is tuned by the overlap extent between the LUMOs of the pyridinium and phenanthridinium subunits of the molecule, which on the other hand is determined by the value of the ρ angle (Figure 9b). Since the HOMO energy does not vary with ρ, the HOMO−LUMO energy gap decreases when ρ does. This effect allows us to rationalize the experimentally observed shift toward longer wavelengths of the visible absorption and emission maxima of pyp viologens with decreasing ρ angles.[1] Moreover, the previously described variation of the ground state

2+/+ redox potential with ρ, as well as the constancy of the *excited state* 2+/+ potential,[1] can also be understood in terms of these calculations. The former potential is expected to correlate with the LUMO energy, since the electron taken up upon reduction of the ground state molecule would enter this orbital. Therefore, a diminution of ρ would result in an increase of this potential, which is the case indeed (−0.07, −0.21, and −0.41 V vs SHE for **1**, **2**, and the $\rho = 94°$ member **3**; see Figure 1 caption, respectively[1]). On the contrary, for the excited state reduction we would expect an electron to enter the singly occupied HOMO orbital, and since the energy of this orbital does not vary with ρ, the excited-state redox potential for pyp viologens with different ρ angles are expected to be essentially the same, as observed experimentally (+2.12, +2.15, and +2.11 V vs SHE for **1**, **2**, and **3**).[1]

As has been demonstrated, the quenching of the drugs fluorescence by DNA is due to an electron transfer from the nucleobases to the singlet excited state of the pyp viologens;[4] this photooxidation has been proposed as the first step in the photosensitized DNA cleavage produced by these molecules.[2] Apart from a large thermodynamic driving force for this electron transfer, expected from the redox potentials of the DNA bases[34] and those of the singlet excited states of the drugs[1] (see above), these calculations explain the observed high efficiency of the photooxidation,[4] since the singly occupied HOMO orbital is centered in the phenanthridinium moiety, and this ring becomes intercalated between two base pairs upon binding to DNA.[1,6] Therefore, a large overlap between the HOMO and the molecular orbitals of the DNA bases occurs in the complex, allowing a very effective electron transfer.

Conclusions

The visible/near-UV absorption band of the pyp viologens results from two different electronic transitions, the lower energy one polarized toward the pyridine ring and the higher energy one parallel to the phenanthridine long axis. A second band, peaking at 250 nm, can be modeled by assuming four additional transitions, having different polarizations. All of the transition moments lie in the phenanthridine plane. The HOMO of the pyp viologens is essentially that of the phenanthridinium moiety, while the LUMO results from the interaction of the two degenerate LUMOs of the pyridinium and phenanthridinium moieties. Therefore, while the LUMO energy is tuned by the pyridinium−phenanthridinium angle, the HUMO energy is constant; this observation allows the rationalization of the spectroscopic and photoredox properties of the different pyp viologens.

Acknowledgment. This work was supported by the Spanish Government Agency DGICYT (Project No. PB92-908) and the Complutense University of Madrid (doctoral fellowship to G.C.). G. C. also acknowledges the European Community for a short-term fellowship within the COST D1 action to visit Chalmers University of Technology. Prof. G. Orellana (Department of Organic Chemistry, Complutense University of Madrid, Spain) is thanked for samples of **1** and **2**, as well as fruitful discussions.

References and Notes

(1) Colmenarejo, G.; Gutiérrez-Alonso, M. C.; Bárcena, M.; Kelly, J. M.; Montero, F.; Orellana, G. *J. Biomol. Struct. Dyn.* **1995**, *12*, 827.
(2) Colmenarejo, G.; Bárcena, M.; Gutiérrez-Alonso, M. C.; Montero, F.; Orellana, G. *FEBS Lett.* **1995**, *374*, 426.
(3) Bárcena, M.; Colmenarejo, G.; Gutiérrez-Alonso, M. C.; Montero, F.; Orellana, G. *Biochem. Biophys. Res. Commun.* **1995**, *214*, 716.
(4) Knapp, C.; Lecomte, J. P.; Kirsch-De Mesmaeker, A.; Orellana, G. *J. Photochem. Photobiol. B:* in press.
(5) Summers, L. A. *The bipyridinium herbicides*; Academic Press: New York, 1980.
(6) Colmenarejo, G.; Montero, F.; Orellana, G. *Anti-Cancer Drug Des.*, in press.
(7) Gutiérrez-Alonso, M. C. Ph.D. Thesis, Universidad Complutense de Madrid, 1996.
(8) Petrow, V.; Wragg, W. R. *J. Chem. Soc.* **1950**, 3516.
(9) Homer, R. F.; Tomlinson, T. E. *J. Chem. Soc.* **1960**, 2498.
(10) Kay, E. R.; Simmons, N. S.; Dounce, A. L. *J. Am. Chem. Soc.* **1952**, *74*, 1724.
(11) Xodo, L. E.; Manzini, G.; Ruggiero, J.; Quadrifoglio, F. *Biopolymers* **1988**, *27*, 1839.
(12) Michl, J.; Thulstrup, E. W. *Spectroscopy with Polarized Light*; VCH Publishers: New York, 1986.
(13) Saupe, A. *Mol. Cryst.* **1966**, *1*, 527.
(14) Nordén, B. *Appl. Spectros. Rev.* **1978**, *14*, 157.
(15) Thulstrup, E. W.; Michl, J.; Eggers, J. H. *J. Phys. Chem.* **1970**, *74*, 3868.
(16) Michl, J.; Thulstrup, E. W.; Eggers, J. H. *J. Phys. Chem.* **1970**, *74*, 3878.
(17) Albinsson, B.; Kubista, M.; Nordén, B.; Thulstrup, E. W. *J. Phys. Chem.* **1989**, *93*, 6646.
(18) Nordén, B.; Kubista, M.; Kurucsev, T. *Q. Rev. Biophys.* **1992**, *25*, 51.
(19) McCaffery, A. J.; Stephens, P. J.; Schatz, P. N. *Inorg. Chem.* **1967**, *6*, 1614.
(20) Cantor, R. C.; Shimmel, P. R. *Biophysical Chemistry*; W. H. Freeman: San Fransicso, 1980; Vo. II, Chapter 8.
(21) Albinsson, B.; Kubista, M.; Sandros, K.; Nordén, B. *J. Phys. Chem.* **1990**, *94*, 4006.
(22) Thulstrup, E. W.; Michl, J. *Elementary Polarization Spectroscopy*; VCH: New York, 1989.
(23) Albinsson, B.; Nordén, B. *J. Am. Chem. Soc.* **1993**, *115*, 223.
(24) Holmén, A.; Albinsson, B.; Nordén, B. *J. Phys. Chem.* **1994**, *98*, 13460.
(25) Houssier, C.; Hardy, B.; Fredericq, E. *Biopolymers* **1974**, *13*, 1141.
(26) Ridley, J. E.; Zerner, M. C. *Theor. Chim. Acta* **1973**, *32*, 111.
(27) Nishimoto, K.; Mataga, Z. *Physik. Chem.* **1957**, *12*, 335.
(28) Baker, J. *J. Comput. Chem.* **1986**, *7*, 385.
(29) Dewar, M. J. S.; Zoebisch, E. G.; Healy, E. F.; Stewart, J. J. P. *J. Am. Chem. Soc.* **1985**, *107*, 3902.
(30) Nordén, B.; Hakansson, R.; Pedersen, P. B.; Thulstrup, E. *Chem. Phys.* **1978**, *33*, 355.
(31) Blacker, A. J.; Jazwinski, J.; Lehn, J.-M. *Helv. Chim. Acta* **1987**, *70*, 1.
(32) Slama-Schwok, A.; Jazwinski, J.; Béré, A.; Montenay-Garestier, T.; Rougée, M.; Hélène, C.; Lehn, J.-M. *Biochemistry* **1989**, *28*, 3227.
(33) Slama-Schwok, A.; Rougée, M.; Ibanez, V.; Geacintov, N. E.; Montenay-Garestier, T.; Lehn, J.-M.; Hélène, C. *Biochemistry* **1989**, *28*, 3234.
(34) Seidel, C. A. M.; Schulz, A.; Sauer, M. H. M. *J. Phys. Chem.* **1996**, *100*, 5541.